Available online at www.sciencedirect.com

jmr&t Journal of Materials Research and Technology

www.jmrt.com.br

Original Article

Growth and characterization of Sm^{3+} doped cerium oxalate single crystals

Minu Mary C[a], *Vimal G*[a], *Kamal P. Mani*[a], *Gijo Jose*[b], *Biju P.R.*[a], *Cyriac Joseph*[a,*], *Unnikrishnan N.V.*[a], *Ittyachen M.A.*[a]

[a] *School of Pure and Applied Physics, Mahatma Gandhi University, Kottayam, India*
[b] *Department of Physics, S B College, Changanassery, India*

ARTICLE INFO

Article history:
Received 25 February 2015
Accepted 27 January 2016
Available online 9 March 2016

Keywords:
Single crystal growth
Rare earth compounds
Oxalates
Phosphors
Microhardness

ABSTRACT

Single crystals of Sm^{3+} doped cerium oxalate decahydrate were synthesized using single diffusion gel technique and the conditions influencing the size, morphology, nucleation density and quality of the crystals were optimized. Highly transparent single crystals of average size 3 mm × 2 mm × 1 mm with well-defined hexagonal morphology were grown during a time period of two weeks. X-ray powder diffraction analysis revealed that the grown crystals crystallize in the monoclinic system with space group $P2_1/c$ as identical with the pure cerium oxalate. The various functional groups of the oxalate ligand and the water of crystallization were identified by Fourier transform infrared spectroscopy. The photoluminescence spectrum of the Sm^{3+} doped cerium oxalate indicated that the Sm^{3+} ions are optically active in the cerium oxalate matrix. The crystal has a strong and efficient orange red emission with a wavelength peak at 595 nm and hence can be effectively used for optical amplification. Microhardness measurements of the crystal revealed that they belong to the soft material category.

1. Introduction

High quality, defect free single crystals have always evoked great attention due to their wide applications in the field of optoelectronics, solid state lasers, remote sensing and medical diagnostics [1–3]. Particular attention can be given to single crystals of trivalent lanthanide compounds owing to their smart optical and spectroscopic properties, which led to potential applications in optoelectronics, lasers, optical amplifiers and in telecommunications [4–6]. The distinctive properties originate from the electronic transitions within the 4f shell of the rare earth ion that is well shielded by 5s and 5p electrons but highly sensitive to the characteristics of the host lattice. Among the rare earth compounds, rare earth oxalates are of special importance because of their interesting luminescent, magnetic and electrical properties [7–10]. Recent investigations on the fluorescence of some rare earth oxalates suggest their potentiality for optical applications [7,11]. Oxalates are also utilized as a precursor for many

* *Corresponding author.*
E-mail: cyriacmgu@gmail.com (C. Joseph).
http://dx.doi.org/10.1016/j.jmrt.2016.01.001

of the technologically important ferroelectric, magnetic and superconducting materials such as $BaTiO_3$, Ni–Co–Zn ferrites and $YBa_2Cu_3O_{7-x}$. [12–14]. Significant attention has been paid to rare earth ion doped crystals, since the dopants play a vital role in enhancing their physical properties. Of the various rare earth ions, Sm^{3+} ions have gained particular attention and are widely investigated in a variety of systems such as bulk crystals, nanocrystals and glasses, due to their high fluorescence quantum yield [5]. Hence, Sm^{3+} ion doped rare earth oxalates deserve special attention and importance.

Here we describe the growth of samarium doped cerium oxalate decahydrate single crystals. Gel method is the only viable method to grow these crystals since oxalates are sparingly soluble in water and decompose before melting, which impose constraints on the use of other conventional techniques. In addition, gel method also allows ease optimization of physical parameters influencing the growth of high quality single crystals. The present work mainly aims to investigate the growth parameters and the effect of Sm^{3+} doping on the optical properties of the cerium oxalate single crystal. The structural and mechanical properties of the crystal are also studied in detail.

2. Experimental

2.1. *Crystal growth*

Cerium nitrate hexahydrate ($Ce(NO_3)_3{\cdot}6H_2O$, 99.9%, CDH), Samarium nitrate hexahydrate ($Sm(NO_3)_3{\cdot}6H_2O$, 99.9%, CDH), oxalic acid dihydrate ($H_2C_2O_4{\cdot}2H_2O$, 99%, Merck) and sodium meta silicate nonahydrate ($Na_2SiO_3{\cdot}9H_2O$, CDH) were used as the starting materials. Sodium meta silicate solution of density 1.03 g/cc was mixed with 1 M oxalic acid to obtain hydrosilica gel of pH 6. The solution was transferred to a test tube of dimension 15 mm in diameter and 150 mm in length to fill half of its volume and then kept undisturbed for 24 h for proper gelation. 0.5 M aqueous solutions of cerium nitrate and samarium nitrate were mixed in stoichiometric proportions and poured gently on the top of the gel column. The reactants slowly diffuse through the gel and react with the oxalic acid already incorporated in the medium. The chemical reaction involved is

$$(2-x)Ce(NO_3)_3{\cdot}6H_2O + xSm(NO_3)_3{\cdot}6H_2O + 3H_2C_2O_4{\cdot}2H_2O \rightarrow Ce_{2-x}Sm_x(C_2O_4)_3{\cdot}10H_2O + 6HNO_3 + 8H_2O$$

where x is taken as 0 and 0.1 for getting pure and 5% Sm doped cerium oxalate decahydrate, respectively. It is observed that whatever be the pH and density of the gel, it cracked as soon as the rare earth solutions were added over the set gel. The concentration of the feed solution was then varied but the observations were the same. To overcome these difficulties neutral gel and double diffusion systems were also undertaken. But the result was not as expected.

Finally, the single diffusion technique was again tried with the feed solution acidified with dilute nitric acid in various proportions. The observation revealed that the presence of nitric acid in the feed solution plays an important role in defining the nature of the precipitation. The density of the precipitation front lowers as the amount of HNO_3 in the feed solution increases. When concentrated HNO_3 was used to acidify the feed solution, there was no precipitation but spherulitic crystals are formed. As the volume of concentrated HNO_3 was further increased, tiny well faceted crystals were obtained. Hence, the acidification of the feed solution was found to be a necessary step in the growth of these groups of crystals.

Morphological changes are exhibited by the crystals due to the variation of the microenvironments like density of the gel, pH of gel, acidity of feed solution and degree of supersaturation. It is observed that crystals taken from different regions of the gel medium show changes in morphology. Fig. 1(a) and (b) shows growth system of Sm^{3+} doped cerium oxalate crystals in silica gel. It is observed that the transparent crystals formed at the bottom of the gel column are thin and have most developed hexagonal prism face while the crystals found at the top of the gel column are of thick rhombic prism morphology. Good quality crystals are found at the bottom of gel column since the availability of the ions is just sufficient for the growth of crystals. Distance of crystallization zone from the gel interface is also different with the acidity of the feed solution. With lower concentration of acid, the heavy nucleation resulted especially at the gel–solution interface as shown in Fig. 1(a). As the acid concentration is increased, nucleation density is decreased and crystallization occurred in a region below gel solution interface, resulting the formation of transparent hexagonal crystals as shown in Fig. 1(b). High concentration of the reactants at the interface of the feed solution and gel surface leads to spontaneous multinucleation resulting to the formation of clustered crystals as shown in Fig. 1(c) and (d). Fig. 1(e) shows the well-developed hexagonal crystal of average size 4 mm × 2 mm × 1 mm grown in the system. Clustered crystal of Sm^{3+} doped cerium oxalate is given in Fig. 1(f) and reveals that these type of crystals are formed by the intergrowth of two or more individual crystals in such a way that they grow together with only part of their similar faces visible.

The effects of the various growth parameters such as density of SMS (sodium meta silicate) solution, pH of the gel, concentration of the reactant and acidity of the feed solution on growth process are manipulated to optimize the conditions of growing good quality crystals. For getting maximum sized, good quality crystals, the optimized conditions are:

Density of the SMS solution – 1.03 g/cc
pH of the gel – 6
Aging of the gel– 24 h
Concentration of inner reactant – 1 M
Concentration of the feed solution – 0.5 M
Acidity of the feed solution – 50% by volume, pH < 2

2.2. *Characterization*

The structure of the grown crystals was identified by X-ray powder diffraction analysis in the range 10–40° using PANalytical X'Pert Pro X-ray diffractometer with Cu-Kα radiation operating at 30 mA, 40 kV. FTIR absorption spectrum of the crystal was recorded using Shimadzu 8400S FTIR spectrometer in the range 400–4000 cm^{-1}. The absorption and emission spectra of the crystals were recorded using Shimadzu UV Probe

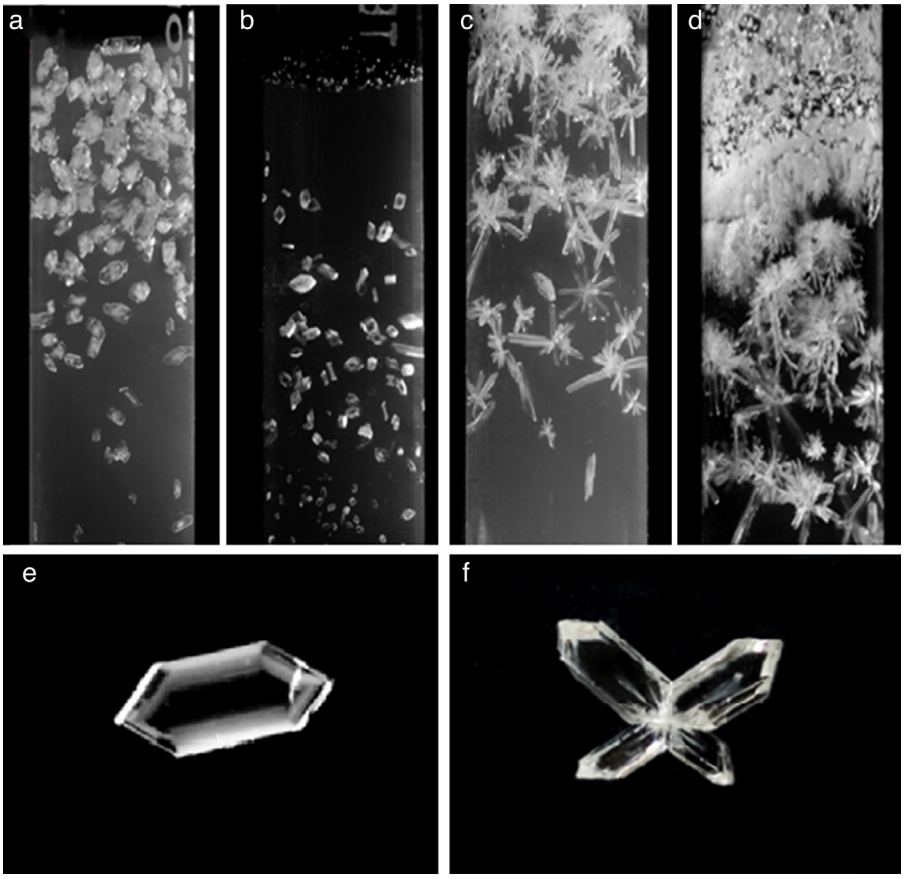

Fig. 1 – (a, b) Growth system of Sm^{3+} doped cerium oxalate crystals with different acid concenteration, (c, d) growth system with clustured morphology, (e, f) morphology of a Sm^{3+} doped cerium oxalate single crystal and clustered crystal, respectively.

spectrophotometer in the wavelength range 250–700 nm and Shimadzu RFPC 5301 spectrofluorophotometer in the range 525–725 nm, respectively. Microhardness of the crystals was measured using a Vicker's microhardness tester.

3. Results and discussion

3.1. *X-ray diffraction analysis*

The XRD patterns of pure $Ce_2(C_2O_4)_3{\cdot}10H_2O$ and Sm^{3+} doped $Ce_2(C_2O_4)_3{\cdot}10H_2O$ single crystals were shown in Fig. 2. All diffraction peaks are matching well with the monoclinic structure of cerium oxalate decahydrate having lattice parameters $a = 11.34$ Å, $b = 9.630$ Å, $c = 10.392$ Å and $\beta = 114.5^{\circ}$ (JCPDS Card No 20-0268) and comparable with the lattice parameters of the $Ln_2(C_2O_4)_3{\cdot}10H_2O$ as reported by Sheng-Hua et al. [15]. Hence, it may be suggested that the grown crystals exhibit monoclinic structure with space group $P2_1/c$ in the decadydrate form. According to Sheng-Hua et al. the structure is composed of two-dimensional networks of edge sharing 1:5:3 coordination polyhedral matching the (020) set of planes. Each lanthanum atom being surrounded by three chelating oxalate groups and three aqua ligands. The intervening space is filled by lattice water molecules disordered over seven major sites. The identical chemical constitution and crystallographic parameters

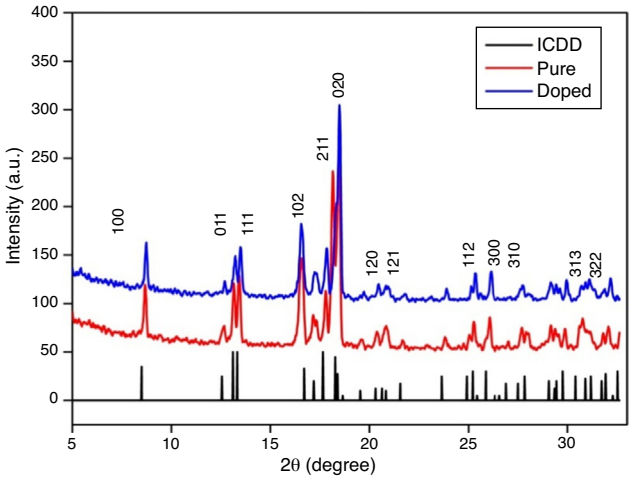

Fig. 2 – X-ray diffractogram of the pure cerium oxalate and Sm^{3+} doped cerium oxalate single crystal.

of rare earth oxalates point to the fact that doped or mixed crystal of any two of them can form by the simple substitutional exchange of rare earth ions. Since the ionic radius and chemical nature of cerium and samarium are comparable with the above-mentioned rare earth elements, one can

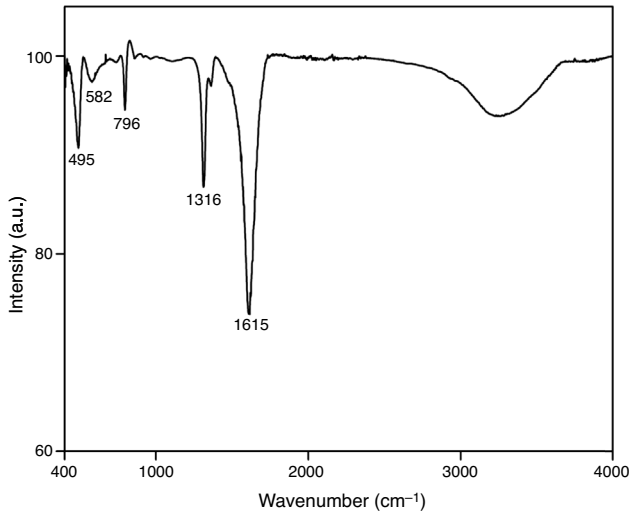

Fig. 3 – Fourier transform infrared spectrum of Sm^{3+} doped cerium oxalate single crystal.

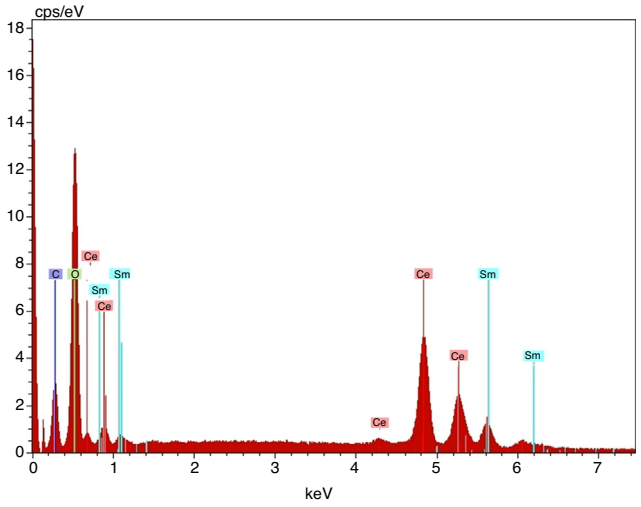

Fig. 4 – Energy dispersive spectrum of Sm^{3+} doped cerium oxalate single crystal.

expect an identical crystal structure for the cerium oxalate and Sm^{3+} doped cerium oxalate single crystals. The close agreement between the 2θ values of single and doped rare earth oxalate crystals support our earlier assumption that the oxalate crystals containing two rare earths of comparable ionic radii can be formed by substitutional exchange of ions and are isostructural with single oxalate crystals. Hence the diffraction peaks observed for $Ce_{2-x}Sm_x(C_2O_4)_3{\cdot}10H_2O$ crystals are indexed assuming that it crystallizes in the monoclinic system with space group $P2_1/c$ having similar structure as that of $Ln_2(C_2O_4)_3{\cdot}10H_2O$ suggested by Sheng-Hua et al.

3.2. *FTIR analysis*

FTIR absorption spectrum of the grown samarium doped cerium oxalate single crystals was given in Fig. 3. The broad envelope extending from 2800 to 3600 cm^{-1} is assigned to be due to the symmetric and asymmetric stretching modes of the water molecules. The strong band appearing in the IR spectrum around 1615 cm^{-1} can be identified as due to the asymmetric stretching vibrations of C—O groups of the $C_2O_4^{2-}$ ions together with the bending mode of water. The strong peak around 1316 cm^{-1} is also assigned to the asymmetric stretching of C—O groups. The strong bands around 495 and 796 cm^{-1} are due to the combined effect of the in-plane deformation mode O—C—O and M—O bond and the weak one around 582 cm^{-1} observed in the spectrum represent the wagging mode [11,16,17]. The FTIR spectroscopic analysis of single crystals of $Ce_{2-x}Sm_x(C_2O_4)_3{\cdot}10H_2O$ confirmed the presence of functional groups associated with the oxalate ligands and the metal–oxygen bond.

3.3. *EDS analysis*

The EDS pattern of Sm^{3+} doped $Ce_2(C_2O_4)_3{\cdot}10H_2O$ crystal was recorded and is shown in Fig. 4. The EDS spectrum confirmed the presence of cerium and samarium in Sm^{3+} doped cerium oxalate single crystal. The atomic percentage of the Ce and Sm is measured to be 13.18 and 0.83, respectively, which supports the doping concentration of Sm^{3+}.

3.4. *Optical properties*

3.4.1. *UV–visible absorption*

The optical absorption spectrum of pure and samarium doped $Ce_2(C_2O_4)_3{\cdot}10H_2O$ crystals are given in Fig. 5(a) and (b), respectively. The broad absorption observed in both the spectra in the UV region is due to the transition from 4f to 5d of Ce^{3+} ions. Sm^{3+} ion will exhibit several overlapped excitation bands from 360 to 500 nm due to its several closely spaced energy levels located in this region [11]. Hence the spectrum of Sm^{3+} doped cerium oxalate exhibits sharp absorption peaks at nUV and visible regions. The transitions in the spectrum are originated from ground state $^6H_{5/2}$ to various multiples of $4f^5$ configurations of Sm^{3+}. The major absorption peaks of Sm^{3+} observed in the spectrum at the wavelength 402, 417, 442, 463, and 479 nm are assigned to the transitions from ground state $^6H_{5/2}$ to the excited states $^4F_{7/2}$, $^4P_{5/2}$, $^4G_{9/2}$, $^4I_{13/2}$ and $^4I_{11/2}$ of Sm^{3+}, respectively [11]. A more enlarged view of the absorption peaks is given in the inset of Fig. 5(b).

3.4.2. *Photoluminescence studies*

The emission spectrum of the pure and Sm^{3+} doped cerium oxalate single crystals when excited at 401 nm is given in Fig. 6(a) and (b). The broad blue-green emission band around 400–500 nm observed in both spectra is originated by the allowed electric dipole transitions ($^2D_{5/2}$, $^2D_{3/2}$)$5d \rightarrow 4f(^2F_{7/2}$, $^2F_{5/2}$) of Ce^{3+} ions. Besides the emission of Ce^{3+} ions, spectrum of Sm^{3+} doped cerium oxalate exhibits sharp emissions at 560, 595 and 643 nm due to the 4f–4f transitions of Sm^{3+} ions. On exciting at 401 nm, the $^4F_{7/2}$ level of Sm^{3+} become excited and after that the electrons nonradiatively relaxes to the $^4G_{5/2}$ level by multiphonon relaxation. Between the $^4F_{7/2}$ and $^4G_{5/2}$ levels there are number of closely spaced higher energy levels that ensure the fast nonradiative decay. The level $^4G_{5/2}$ has

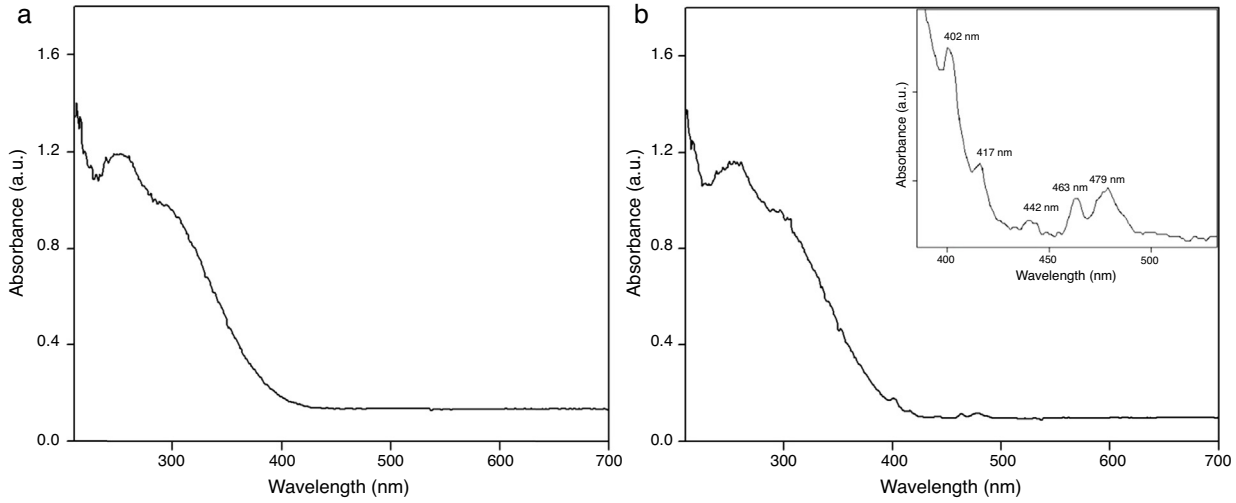

Fig. 5 – UV–Vis absorption spectrum of (a) cerium oxalate single crystal and (b) Sm^{3+} doped cerium oxalate single crystal.

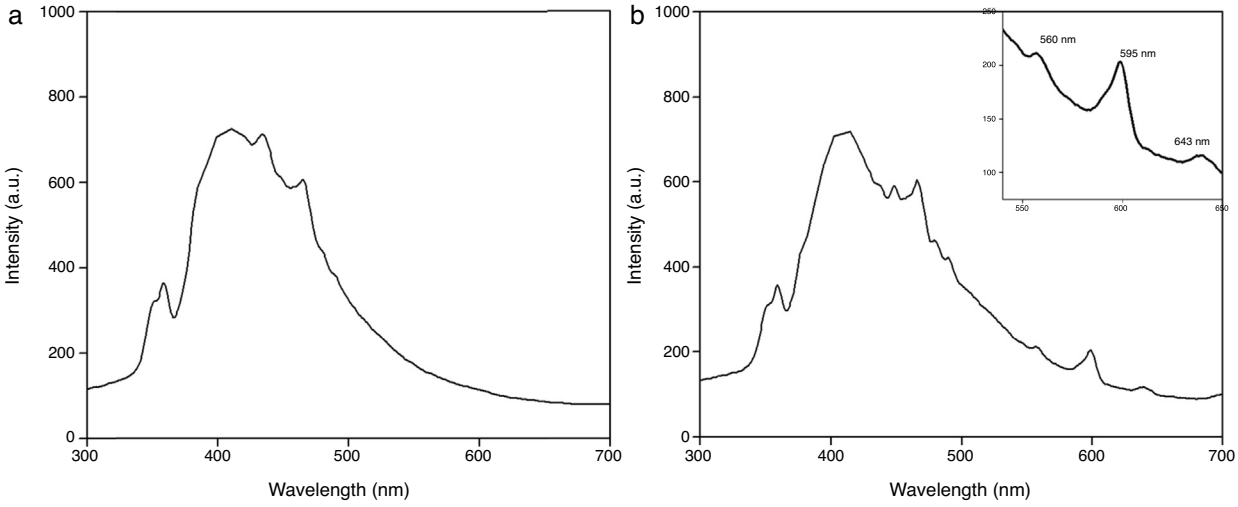

Fig. 6 – Photoluminescence spectrum of (a) cerium oxalate single crystal and (b) Sm^{3+} doped cerium oxalate single crystal.

sufficient energy gap higher than five phonons with respect to the next lower level. This encourages radiative transition to the ground state. Hence the emission spectrum of Sm^{3+} doped cerium oxalate exhibits three emission transitions from the excited level $^4G_{5/2}$ of Sm^{3+} ions to lower ground levels $^6H_{5/2}$, $^6H_{7/2}$ and $^6H_{9/2}$ corresponds to 560 nm, 595 nm and 643 nm, respectively [5]. The emission spectrum reveals that the emission from $^4G_{5/2}$ to $^6H_{7/2}$ at 595 nm has maximum intensity and resulting strong emission in the orange region.

3.5. *Microhardness measurements*

Perfectly plane single crystals of Sm^{3+} doped cerium oxalate were selected for the microhardness measurements. Indentation was carried out, using a Vickers microhardness tester (Leitz Wetzlar) for various loads ranging from 5 to 100 g. The duration of the indentation time was kept constant at 30 s and in all measurements, the distance between the two indentations was kept 10 times greater than the diagonal length of the indentation mark in order to avoid any mutual influence of the indentations. For each load, several indentations were done to calculate the microhardness. The hardness number H_v of the crystal was calculated using the equation:

$$H_v = \frac{1.854P}{d^2}\ \mathrm{kg/mm^2} \quad (1)$$

The increase in hardness with load is primarily caused by the work hardening of the surface layers. Fig. 7 shows the variation of microhardness H_v against applied load in the case of $Ce_{2-x}Sm_x(C_2O_4)_3{\cdot}10H_2O$ crystals. It was found that as load increases, microhardness increases initially and then due to the rearrangements of dislocations and mutual interactions between them, the value of microhardness becomes almost constant above a particular load.

Inset of Fig. 7 shows the variation of $\log P$ vs $\log d$. Meyer's index number was calculated from Meyer's law, which relates the load and indentation diagonal length.

$$P = kd^n \quad (2)$$

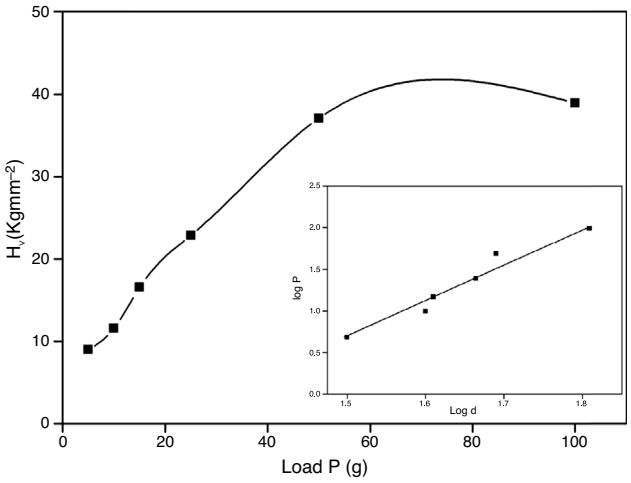

Fig. 7 – Variation of microhardness with applied load and plot of log *P* as a function of log *d* (inset).

$$\log P = \log k + n \log d \quad (3)$$

where k is the material constant and n is Meyer's index (or work-hardening coefficient). The above relation indicates that H_v should increases with P if $n > 2$ and decrease with P when $n < 2$. The relation can be plotted as a linear function that provides n from the slop. On the basis of careful investigation on various substances, Kalainathan et al. had shown that the values of n come out to be 1–1.6 for hard materials and more than 1.6 for soft ones [18]. The value of 'n' calculated from the graph is 4.2 ± 0.5 which suggest that $Ce_{2-x}Sm_x(C_2O_4)_3{\cdot}10H_2O$ single crystal belongs to soft-material category.

4. Conclusion

The present work reports the growth and characterization of samarium doped cerium oxalate single crystals. Hydrosilica gel is found to be the best medium for growing good quality oxalate crystals of rare earths. Pure and well faceted single crystals of very good quality are obtained as a result of controlled diffusion of rare earth ions through hydrosilica gel enriched with oxalate ions. The habits of the grown crystals depend to a very large extent on the gel structure, nature and molarity of the acid used, strength and purity of sodium meta silicate, pH, environmental temperature, etc. The X-ray powder diffraction analysis of pure and doped cerium oxalate crystals revealed that both crystals are isostructural and belong to the monoclinic system with space group $P2_1/c$. The infrared (IR) absorption spectrum of Sm^{3+} doped cerium oxalate establishes the presence of oxalate $(C_2O_4)^{2-}$ ions and water of hydration. Energy dispersive X-ray spectroscopy confirmed the presence of cerium and samarium in the doped crystals. Fluorescence spectrum of $Ce_{2-x}Sm_x(C_2O_4)_3{\cdot}10H_2O$ exhibits broad emission of Ce^{3+} ions and sharp emissions of Sm^{3+} in the blue and red regions, respectively. Among the emission bands, the transition $^4G_{5/2} \rightarrow {}^6H_{7/2}$ at 598 nm has the maximum intensity and the emission can be effectively used for optical amplification. Microhardness measurements of the single crystal revealed that the grown crystals belong to the soft material category.

Conflicts of interest

The authors declare no conflicts of interest.

Acknowledgments

The authors are thankful to UGC (Govt. of India) and DST (Govt. of India) for the financial assistance through SAP-DRS (No. F.530/12/DRS/2009 (SAP-1)) and DST-PURSE (SR/S9/Z-23/2010/22) (C,G) programs, respectively. The authors Vimal G and Kamal P Mani are thankful to University Grants Commission, Govt. of India for the award of RFSMS fellowship.

REFERENCES

[1] Ogorodnikov IN, Pustovarov VA, Goloshumova AA, Isaenko LI, Yelisseyev AP, Pashkov VM. A luminescence spectroscopy study of SrI_2:Nd^{3+} single crystals. J Lumin 2013;143:101–7.
[2] Elizabeth A, Joseph C, Paul I, Ittyachen MA, Mathew KT, Lonappan A, et al. Microwave studies on double rare earth oxalate crystals. Mater Sci Eng A 2005;391:43–50.
[3] Misoguti L, Varela AT, Nunes FD, Bagnato VS, Melo EEA, Filho JM, et al. Optical properties of L-alanine organic crystals. Opt Mater 1996;6:147–52.
[4] Eliseeva SV, Bunzli JCG. Rare earths: jewels for functional materials of the future. New J Chem 2011;35:1165–76.
[5] Vimal G, Mani KP, Jose G, Biju PR, Joseph C, Unnikrishnan NV, et al. Growth and spectroscopic properties of samarium oxalate single crystals. J Cryst Growth 2014;404:20.
[6] Brandt C, Matrosov V, Petermann K, Huber G. In-band fiber-laser-pumped Er:YVO_4 laser emitting around 1.6 μm. Opt Lett 2011;36:1188–90.
[7] Thomas V, Elizebeth A, Thomas H, Jose G, Unnikrishnan NV, Joseph C, et al. Studies on the growth and optical characterization of dysprosium praseodymium oxalate single crystals. J Optoelectron Adv Mater 2005;7:2687–92.
[8] Que W, Kam CH. Effects of erbium oxalate content and temperature on green up-conversion luminescence of erbium oxalate nanoparticles/titania/ormosil composite thin films. Opt Commun 2002;206:211–6.
[9] Joseph C, Varghese G, Ittyachen MA. Growth and characterization of mixed neodymium praseodymium oxalate decahydrate crystals in silica gel. Cryst Res Technol 1995;30:159–64.
[10] Ang WA, Gupta N, Prasanth R, Madhavi S. High-performing mesoporous iron oxalate anodes for lithium-ion batteries. ACS Appl Mater Interfaces 2012;4:7011–9.
[11] Vimal G, Mani KP, Biju PR, Joseph C, Unnikrishnan NV, Ittyachen MA. Synthesis, structural and spectroscopic investigations of nanostructured samarium oxalate crystals. Spectrochim Acta A 2014;122:624–30.
[12] Jung W, Min B, Park J, Yoon DH. Formation mechanism of barium titanate by thermal decomposition of barium titanyl oxalate. Ceram Int 2011;37:669–72.
[13] Ghodake JS, Kamble RC, Kulkarni SD, Sawant SR, Suryavanshi SS. Complex permeability studies of Ni–Co–Zn ferrites synthesized by an oxalate precursor method. Smart Mater Struct 2009;18:125009–17.
[14] Shter GE, Grader GS. YBCO oxalate coprecipitation in alcoholic solutions. J Am Ceram Soc 1994;77:1436–40.

[15] Sheng-Hua H, Zhou GD, Mak TCW. Crystal structure of lanthanum(III) oxalate decahydrate. J Crystallogr Spectrosc Res 1991;21:127–31.
[16] Joseph C, Ittyachen MA, Raju KS. Some structural aspects of neodymium praseodymium oxalate single crystals grown in hydro silica gel. Bull Mater Sci 1997;20:37–48.
[17] Mancilla N, D'Antonio MC, González-Baró AC, Baran EJ. Vibrational spectra of lead(II) oxalate. J. Raman Spectrosc 2009;40:2050–2.
[18] Kalainathan S, Jagannathan K. Mechanical and surface analysis of stilbazolium tosylate derivative crystals. J Cryst Growth 2008;310:2043–9.